

Indo-Pacific remote forcing in summer rainfall variability over the South China Sea

Zhuoqi He · Renguang Wu

Received: 30 December 2013 / Accepted: 11 March 2014 / Published online: 22 March 2014
© Springer-Verlag Berlin Heidelberg 2014

Abstract This study investigates summer rainfall variability in the South China Sea (SCS) region and the roles of remote sea surface temperature (SST) forcing in the tropical Indian and Pacific Ocean regions. The SCS summer rainfall displays a positive and negative relationship with simultaneous SST in the equatorial central Pacific (ECP) and the North Indian Ocean (NIO), respectively. Positive ECP SST anomalies induce an anomalous low-level cyclone over the SCS-western North Pacific as a Rossby-wave type response, leading to above-normal precipitation over northern SCS. Negative NIO SST anomalies contribute to anomalous cyclonic winds over the western North Pacific by an anomalous east–west vertical circulation north of the equator, favoring more rainfall over northern SCS. These NIO SST anomalies are closely related to preceding La Niña and El Niño events through the “atmospheric bridge”. Thus, the NIO SST anomalies serve as a medium for an indirect impact of preceding ECP SST anomalies on the SCS summer rainfall variability. The ECP SST influence is identified to be dominant after 1990 and the NIO SST impact is relatively more important during 1980s. These Indo-Pacific SST effects are further investigated by conducting numerical experiments with an atmospheric general circulation model. The consistency between the numerical experiments and the observations

enhances the credibility of the Indo-Pacific SST influence on the SCS summer rainfall variability.

Keywords South China Sea summer rainfall · North Indian Ocean SST · Equatorial central Pacific SST · Indirect influence of Pacific SST · Numerical experiments

1 Introduction

As part of the eastern Indian-western Pacific Ocean warm pool, the South China Sea (SCS) climate displays a pronounced year-to-year variability. Anomalous convection and associated heating over the SCS can affect climate over East and Southeast Asia (Ding 1994a; Li and Zhang 1999). The climate variability over the SCS is not only connected to the variability of East Asian and Indonesia–Australian monsoons, it also plays an important role in connecting the variability among these monsoons (Tao and Chen 1987). Previous studies indicate that the SCS is as a pathway for moisture transport from the North Indian Ocean and the Southern Hemisphere to China (Tao and Chen 1987; Ding 1994b; Zhou and Yu 2005; Wu et al. 2006). It is suggested that the SCS serves as a medium linking the remote forcing of El Niño–Southern Oscillation (ENSO) and tropical Indian Ocean to regional climate in the surrounding regions (Wang et al. 2000; Xie et al. 2009; Wu et al. 2010). The SCS is also a region of activity of tropical cyclones/typhoons that pose a great threat to coastal southern China (Wang et al. 2007; Chen et al. 2012). Thus, it is important to understand the factors and processes of the SCS climate variability.

The SCS climate variability may subject to both regional air–sea interaction and remote forcing. He and Wu (2013a) documented seasonal air–sea interaction processes

Z. He · R. Wu (✉)
Institute of Space and Earth Information Science, The Chinese University of Hong Kong, Shatin, Hong Kong SAR, China
e-mail: renguang@cuhk.edu.hk

R. Wu
Shenzhen Research Institute, The Chinese University of Hong Kong, Shenzhen, China

in the SCS region. He and Wu (2013b) investigated the air–sea relationship on interannual time scale in the SCS region and evaluated the performance of climate models in simulating the air–sea relationship. They found strong seasonal dependence of regional air–sea relationship. The purpose of this study is to investigate summer rainfall variability in the SCS region and the roles of remote forcing of the tropical Indian and Pacific Ocean regions.

As one of the strongest signal in short-term climate variability, ENSO exerts a significant influence on climate variability in many regions over the world, including the SCS region (Wang and Zhang 2002; Liu et al. 2004; Wang et al. 2006; Chen et al. 2014a). Positive sea surface temperature (SST) anomalies appear in the SCS about 5 months after the peak of an El Niño event (Klein et al. 1999). This surface warming in the SCS was attributed to an increase in net surface heat flux entering the ocean that is related to the reduced cloud cover and increased downward solar radiation due to enhanced subsidence during El Niño events (Klein et al. 1999; Wang et al. 2006). Due to its modulation on atmospheric circulation, convection, and SST in the SCS, the ENSO plays an important role in the interannual variability of the summer monsoon onset over the SCS and western North Pacific (Wu and Wang 2000).

El Niño–Southern Oscillation can influence regional climate either directly or indirectly. For example, Wu et al. (2012) revealed different types of ENSO influences on the Indian summer monsoon, including both the indirect influence of preceding winter SST anomalies in the eastern equatorial Pacific, and the direct influence of concurrent summer equatorial Pacific SST anomalies. Wu and Kirtman (2011) pointed out different processes connecting the ENSO and the Caribbean Sea summer rainfall variability. The direct influence of ENSO on regional climate can be explained by atmospheric circulation changes. The delayed (indirect) impacts of ENSO may be closely linked to regional air–sea interactions. Wang et al. (2000, 2003) indicated that a positive thermodynamic feedback between surface heat flux and SST in the western North Pacific maintains regional SST anomalies and provides a delayed impact of ENSO on the East Asian climate. Although there have been a few studies on the influences of ENSO on the South China Sea climate variability (e.g., Liu et al. 2004; Wang et al. 2006), the previous studies have not separated the direct and indirect impacts of ENSO.

Recent studies suggest important impacts of tropical Indian Ocean SST anomalies on circulation and climate over the SCS–the Philippine Sea (Yang et al. 2007; Li et al. 2008; Xie et al. 2009; Wu et al. 2010, 2014). El Niño-induced tropical Indian Ocean warming forces a Kelvin-wave response that extends into the western Pacific. The resultant Ekman divergence north of the equator leads to

the suppression of convection and the development of an anomalous anticyclone over the western North Pacific (Xie et al. 2009). An alternative explanation for the influence of the tropical Indian Ocean warming on the SCS–Philippine Sea circulation is via an anomalous east–west vertical circulation (Wu et al. 2010).

These previous studies have focused on the impact of either the Pacific or Indian Ocean SST anomalies on the SCS climate. They, however, have not compared the individual roles of tropical Indian and Pacific Ocean SST anomalies in the SCS climate variability. There are still questions that have not been addressed. For example, SST warming in the equatorial central and eastern Pacific in a mature El Niño event may have an indirect influence on the SCS rainfall in the following summer. Meanwhile, the Pacific SST anomalies in boreal summer may have a direct impact on the SCS summer rainfall. The previous studies have not distinguished these two different types of Pacific SST influences. Moreover, during boreal summer, SST anomalies in both the Pacific and Indian Ocean can exert simultaneous impacts on the SCS summer rainfall through atmospheric teleconnections. Previous studies have not compared the individual and combined effects of the Pacific and Indian Ocean SST anomalies. The present study is to differentiate the synchronous and delayed ENSO influences on the summer rainfall variability in the SCS region and to investigate the respective processes of the Pacific and Indian Ocean SST influences.

The organization of the text is as follows. Section 2 describes the data and methods used in the present study. In Sect. 3, we present the summer rainfall variability in the SCS and select typical years to distinguish the Indian and Pacific Ocean SST influence cases. Different cases of the Indian and Pacific SST influences and the corresponding processes are analyzed based on composite in Sect. 4. Section 5 investigates the respective contributions of the Pacific and Indian Ocean SST anomalies through numerical experiments. Summary and discussions are presented in Sect. 6.

2 Datasets and methods

The National Oceanic and Atmospheric Administration (NOAA) optimum interpolation (OI) version 2 monthly mean SST (Reynolds et al. 2002) is used in present study. This dataset, available at <http://www.esrl.noaa.gov/psd/>, is on a $1^\circ \times 1^\circ$ grid and covers the period of December 1981 to present. The present study uses the Global Precipitation Climatology Project (GPCP) Version 2.2 monthly precipitation dataset (Adler et al. 2003; Huffman

et al. 2009), which is provided by the NOAA/OAR/ESRL PSD (<http://www.esrl.noaa.gov/psd/>). The GPCP precipitation has a resolution of $2.5^\circ \times 2.5^\circ$ and is available from January 1979 to present. The present study uses monthly mean net surface shortwave radiation and latent heat fluxes from the Woods Hole Oceanographic Institute (WHOI) Objectively Analyzed Air–sea Fluxes (OAFflux) project (Yu et al. 2008, <http://oafux.whoi.edu>). The shortwave radiation, originally derived from the International Satellite Cloud Climatology Project (ISCCP) (Zhang et al. 2004), has been re-gridded to 1° grid and covers the period from July 1983 to December 2009. The present study uses monthly mean horizontal winds and vertical p-velocity from the National Centers for Environmental Prediction–Department of Energy (NCEP–DOE) Reanalysis 2, which are provided by the NOAA/OAR/ESRL Physical Science Department (PSD) from the web site at <http://www.esrl.noaa.gov/psd/> (Kanamitsu et al. 2002). The reanalysis two dataset is available from 1979 to the present on a $2.5^\circ \times 2.5^\circ$ grid.

The atmosphere component of the Community Earth System Model (CESM) is used in the present study. Composed of five component models simultaneously simulating the Earth's atmosphere, ocean, land, land-ice, and sea-ice, plus one central coupler component, CESM allows conducting fundamental research about the Earth's past, present, and future climate states (Vertenstein et al. 2011). The Community Atmosphere Model, version 5.1.1 (CAM5.1.1), was released as part of the atmospheric component of the CESM, version 1.0.4. It is one of the latest in a series of global atmospheric models whose development is guided by the Atmosphere Model Working Group (AMWG) of the CESM project. CAM is used both as the atmospheric component of the CESM, and as a stand-alone model in which the atmosphere is coupled to an active land model, a thermodynamic only sea ice model, and a data ocean model (Eaton 2012). The stand-alone model is suitable for estimating the equilibrium response to external forcings, such as examining the response of the atmospheric circulation to changes in SST. It can also be used to study the interactions of the atmosphere, ocean, sea ice, and land surface on seasonal to millennial time scales (Collins et al. 2006). Model details can be referred to Eaton (2012) and Vertenstein et al. (2011).

A linear interpolation is used to convert all the variables to 1° resolution for the calculation of correlation and regression. The correlation, regression, composite, and empirical orthogonal function (EOF) analysis are performed based on seasonal mean anomalies. The climatology of the shortwave radiation is derived based on the period of 1984–2009 and other variables on the period of 1983–2012 when all the observational datasets are available.

3 Different types of SST influences on the SCS summer rainfall variability

In this section, we discuss the relationship between the SCS summer rainfall and large-scale atmospheric and oceanic variables to detect the regions where the SST anomalies may contribute to the variability of the SCS summer rainfall. Figure 1 shows the dominant spatial pattern of the summer (June–July–August, JJA) precipitation anomaly in the SCS domain and its corresponding Principal Component (PC) obtained by an EOF analysis. The pattern agrees with Wu et al. (2014). The leading mode represents well the summer rainfall variability over the SCS, accounting for about 37 % of total interannual variance. The second and third modes explain about 19 and 12 % of total variance, respectively (figures not shown). The leading spatial pattern shows an opposite-sign distribution in the south–north direction with the largest loading in northern SCS. The corresponding PC displays interannual variations with approximately a 4-year period.

To identify the remote forcing related to the variability of JJA precipitation in the SCS, simultaneous regression maps with respect to the leading PC of SCS summer precipitation are shown in Fig. 2. Different local SST–precipitation relationships are found in different regions. A positive relationship between local SST and precipitation can be seen in the equatorial Pacific between 165°E and 120°W , the tropical North Pacific between 150°E and 180°E , the North Indian Ocean between 50°E and 100°E , and southern SCS–the Maritime Continent (MC)–north of Australia. This indicates local SST forcing of precipitation in these regions (Wu et al. 2006; Wu and Kirtman 2007). In northern and central SCS and the western North Pacific over 120°E – 150°E , 5°N – 20°N , there is a negative relationship between local SST and precipitation, which signifies an atmospheric forcing of the SST variation (Wu et al. 2006b; Wu and Kirtman 2007). Here, we note two important regions with significant SST anomalies. One is the equatorial central Pacific (ECP), and the other is the North Indian Ocean (NIO) (Fig. 2b). Above-normal SCS summer rainfall (Fig. 2a) corresponds to positive SST anomalies in the ECP and negative SST anomalies in the NIO, respectively (Fig. 2b). Positive SST anomalies in the ECP and negative SST anomalies in the NIO may induce anomalous heating and cooling, modulating circulation and precipitation over the SCS. From Fig. 2, anomalous low-level cyclonic winds are overlaid by anomalous upper-level anticyclonic winds over the SCS–western North Pacific, leading to positive precipitation anomalies in this region (Fig. 2a). After precipitation anomalies are induced, associated anomalous heating may amplify the cyclonic and anti-cyclonic winds through circulation–precipitation coupling. The low-level anomalous cyclone features a Rossby-

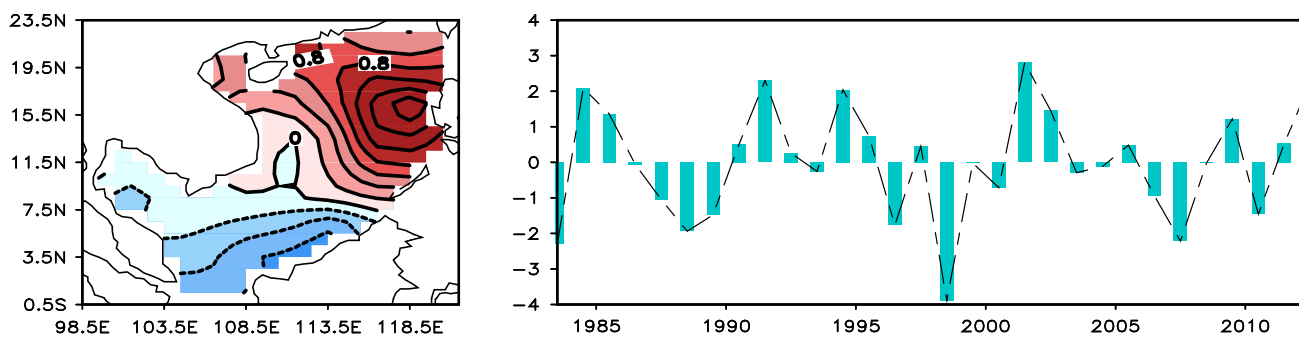


Fig. 1 The 1st EOF mode and the corresponding principal component (PC) of the SCS summer precipitation anomalies (mm/day) for the period of 1983–2012

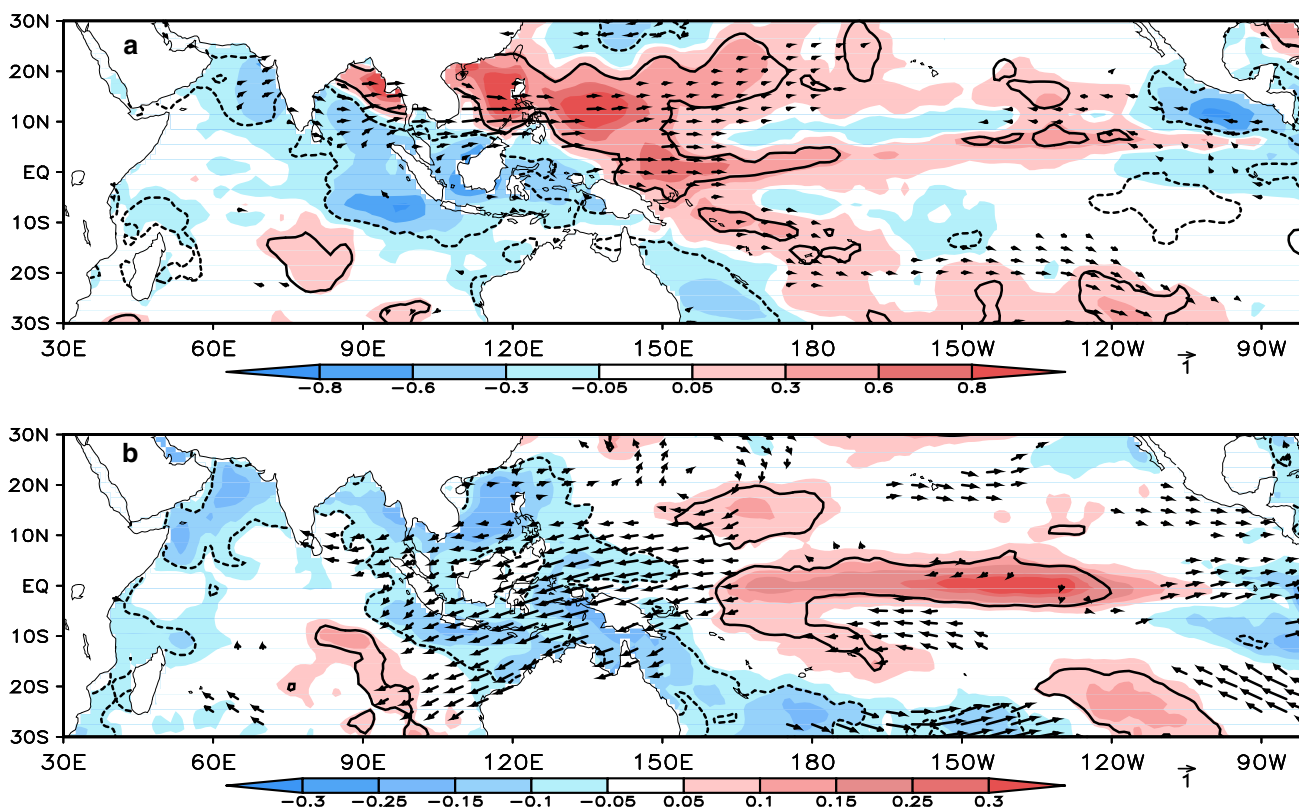


Fig. 2 Regression with respect to the leading PC of SCS summer rainfall: precipitation (shading, mm/day) and wind (vector, m/s) anomalies at 850 hPa (a), SST (shading, °C) and wind (vector, m/s) anomalies at 200 hPa (b) for the period of 1983–2012. Thick contours

indicate that the correlations are statistically significant at the 90 % confidence level. Only wind anomalies that are significant at the 90 % confidence level are plotted

wave type response to positive SST anomalies in the ECP as well as a Kelvin wave type response to negative SST anomalies in the NIO. The above-normal rainfall, in turn, leads to SST cooling in the SCS.

In this study, NOAA OI 1/4 Degree Daily SST V2 Dataset and the Tropical Rainfall Measuring Mission (TRMM) Precipitation Data with a horizontal $0.25^\circ \times 0.25^\circ$ resolution are also employed for verification (figures not shown). A south-north opposite-sign distribution of the SCS JJA

rainfall anomaly in the dominant EOF mode is detected using the TRMM data. The positive (negative) relationship between the SCS summer rainfall and the SST in both the equatorial central Pacific and the central-western North Pacific (the North Indian Ocean and the SCS region), which is calculated by the NOAA OI 1/4 high-resolution data, can be found as well. The results show highly consistency among different datasets, which enhances the reliability of the analysis in this study.

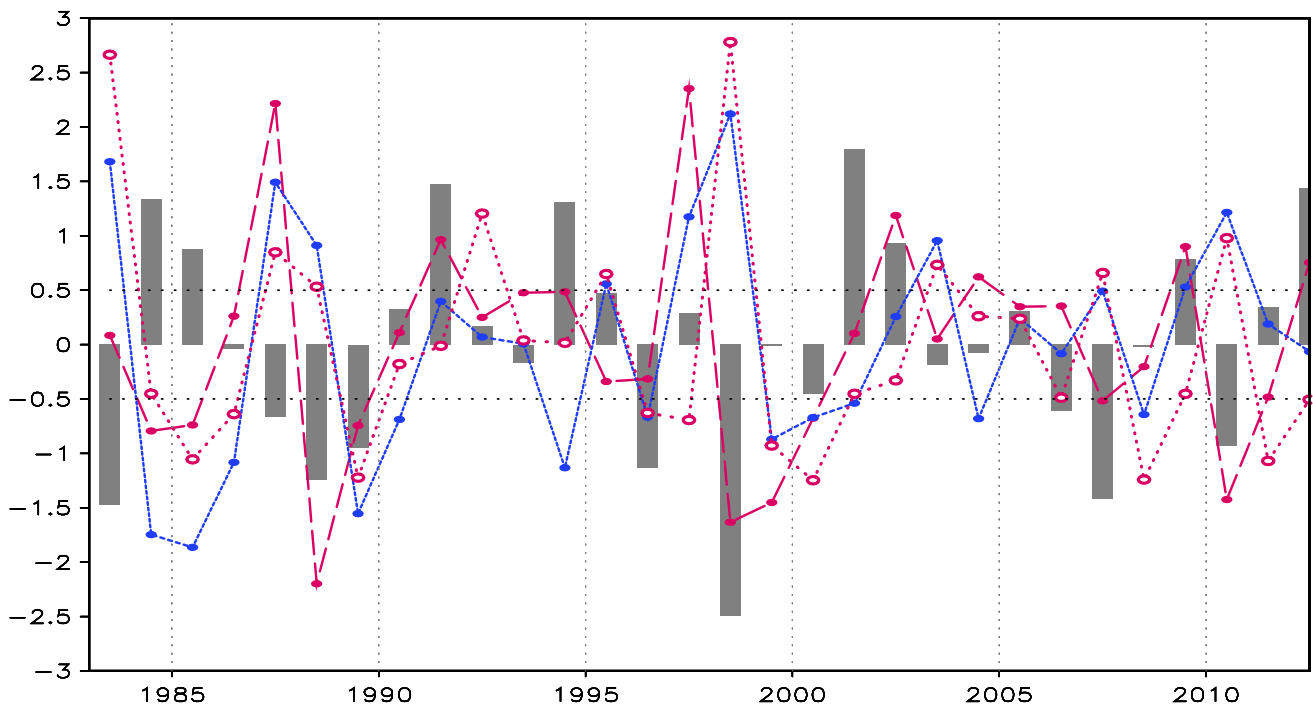


Fig. 3 Time series of the leading PC of SCS summer rainfall (*gray-bar*, mm/day), the JJA equatorial central Pacific SST anomalies (*red-dashed*, °C), the JJA North Indian Ocean SST anomalies (*blue-*

dashed, °C), the preceding DJF equatorial eastern Pacific SST anomalies (*red-dotted*, °C) for the period of 1983–2012. The 0.5 standard deviation is the criterion for an anomalous year

Do the SST anomalies in the above two regions contribute coherently and individually to the variability of summer rainfall in the SCS? To examine the ECP and NIO SST influence, we compare in Fig. 3 year-to-year variations of the normalized area-mean SST anomalies with the leading PC to identify different cases. The ECP SST (red, dashed) is the average of SST anomalies over the region of 170°W–120°W and 5°S–5°N, and the NIO SST (blue, dashed) is the average of SST anomalies over the region of 50°E–90°E, 5°N–20°N. There is obviously a simultaneous positive relationship between the ECP SST and the leading PC with a correlation coefficient of 0.41, and a negative relationship between the NIO SST and the leading PC with a correlation coefficient of -0.46 . This conforms that when the SST in the ECP is higher and that in the NIO lower, northern SCS experiences more rainfall in summer.

Detailed relationship between SCS rainfall and ECP and NIO SST anomalies is given in Table 1 that lists the abnormal years when both the leading PC and the ECP and/or NIO SSTs are significantly anomalous during the period from 1983 to 2012. The criterion for an abnormal (significant anomalous) year is that the magnitudes of both the normalized leading PC and ECP (NIO) SST anomaly exceed the 0.5 standard deviation. For the ECP SST-SCS summer rainfall relationship, here denoted as the ECP case, there are ten abnormal years with a same-sign ECP SST-SCS rainfall relationship (including positive SST—positive

rainfall and negative SST—negative rainfall anomalies) and three abnormal years with an opposite-sign relationship (SST and rainfall have opposite anomalies). For the NIO SST-SCS rainfall relationship (denoted as the NIO case), there are 10 years with an opposite-sign relationship and 4 years with a same-sign relationship.

Comparing the ECP SST and the NIO SST influences, we further distinguish three types of cases (lower part of Table 1): (1) the ECP-only case in which there is a same-sign relationship between the SCS rainfall and the ECP SST anomalies while the NIO SST-SCS rainfall relationship is insignificant; (2) the NIO-only case in which there is an opposite-sign SCS rainfall-NIO SST relationship and the ECP SST-SCS rainfall relationship is insignificant; (3) the co-existing case with both a same-sign ECP SST-SCS rainfall relationship and an opposite-sign NIO SST-SCS rainfall relationship. According to Table 1, there are 5 years belonging to the ECP-only cases (1989, 1991, 2002, 2009, and 2012), 5 years belonging to the NIO-only cases (1983, 1984, 1985, 1987, and 2001), and 5 years belonging to the co-existing cases (1988, 1994, 1998, 2007, 2010). The temporal distribution of the above cases indicates that the ECP cases tend to be dominant after 1990 and the NIO cases are relatively more during 1980s. The processes of the SST influence on the SCS summer rainfall will be discussed in the next section for the ECP-only cases, the NIO-only cases, and the co-existing cases, respectively.

Table 1 Relationship between the leading PC of SCS JJA rainfall and JJA ECP SST, JJA NIO SST, DJF EEP SST for the period 1983–2012

Index	Year																	Total
	83	84	85	87	88	89	91	94	95	96	98	01	02	07	09	10	12	
SCS rainfall	–	+	+	–	–	–	+	+	+	–	–	+	+	–	+	–	+	10
JJA ECP SST		–	–	+	–	–	+	+			–		+	–	+	–	+	10
JJA NIO SST	+	–	–	+	+	–		–	+	–	+	–		+	+	+		10
DJF EEP SST	+	–	–	+	+	–			+	–	+	–		+	–	+	–	11
ECP only						✓	✓						✓		✓		✓	5
NIO only	✓	✓	✓	✓								✓						5
Co-exist					✓			✓			✓			✓		✓		5

“+”/“–” represents significant positive/negative leading PC, ECP SST, NIO SST or preceding DJF EEP SST anomalies based on the criterion of 0.5 standard deviation. Bold stands for the years with a same-sign (opposite-sign) ECP (NIO or EEP) SST-SCS summer rainfall relationship. “ECP only” (“NIO only”) with “✓” denotes the years with a same-sign (opposite-sign) relationship between SCS rainfall and ECP SST (NIO SST) while NIO SST (ECP SST)-SCS rainfall relationship is insignificant. “Co-exist” with “✓” denotes the years with both significant SCS rainfall-ECP SST relationship and significant SCS rainfall-NIO SST relationship

4 The influence of ECP and NIO SST anomalies

In this section, we perform composite analyses corresponding to the different cases selected in Sect. 3. We discuss firstly the ECP-only cases, followed by the NIO-only cases, and finally the co-existing cases. The composite anomalies are calculated as the difference of anomalies with positive leading PC minus those with negative leading PC, hereafter referred to as “more minus less composite”. The one sample *t* test is employed for the significance test in Figs. 4, 5 and 8.

4.1 The ECP SST influence

Five years (1989, 1991, 2002, 2009, and 2012) are used in composite analysis for the ECP-only cases. Figure 4a, b displays the corresponding composite anomalies of JJA mean precipitation, SST, winds at 850 and 200 hPa. During these years, positive SST anomalies are observed in the equatorial Pacific and tropical Indian Ocean (Fig. 4b). The wind anomalies feature a Rossby-wave type response to the equatorial Pacific SST anomalies. An anomalous low-level cyclone is induced to the northwest of anomalous warming over the equatorial Pacific and extends to northern SCS with low-level westerly anomalies lying north of the equator between 90°E and 160°E and easterly anomalies over southern China (Fig. 4a). Accordingly, positive precipitation anomalies develop along the equatorial central and western Pacific and the rain belt extends to northern SCS accompanying the extension of the cyclonic wind anomalies. These precipitation anomalies in turn feed back to the local SST by reducing incoming shortwave radiation and enhancing upward surface latent heat flux (figures not shown). The cloud-radiation effect working with the wind-evaporation effect leads to lower SST in the SCS and the Philippine Sea (Fig. 4b).

Another feature to note is the negative SST anomalies around the MC (Fig. 4b) that are accompanied by below-normal precipitation and low-level anticyclonic wind anomalies (Fig. 4a). These negative SST anomalies contrast with positive SST anomalies in the equatorial central and eastern Pacific, leading to an east–west anomaly pattern. This SST anomaly pattern induces an anomalous Walker circulation with anomalous low-level westerlies and upper-level easterlies over the equatorial Pacific, anomalous upward motion and above-normal precipitation over the ECP and anomalous downward motion and below-normal precipitation over the MC. The anomalous cooling over the MC is conducive to anomalous upward motion and above-normal precipitation over the SCS via an anomalous meridional vertical circulation (Fig. 4c) (Wu et al. 2012; Chen et al. 2014b). Hence, both positive ECP SST anomalies and negative MC SST anomalies contribute to more precipitation over the northern SCS.

4.2 The NIO SST influence as a medium of ENSO impact

Figure 5a, b show the more minus less composite anomalies of JJA mean precipitation, SST, 850 hPa wind and 200 hPa wind for the NIO-only case (1983, 1984, 1985, 1987, and 2001). Significant negative SST anomalies are present in the NIO (Fig. 5b), accompanied by below-normal precipitation (Fig. 5a). Significant negative SST anomalies are seen in the equatorial eastern Pacific, accompanied by below-normal precipitation over the ECP. The wind anomalies over the ECP, however, are weak. Low-level cyclonic wind anomalies are observed over northern SCS—the western North Pacific, which contributes to positive precipitation anomalies (Fig. 5a). Note that there are positive SST anomalies in the North Pacific between 150°E and 170°W (Fig. 5b).

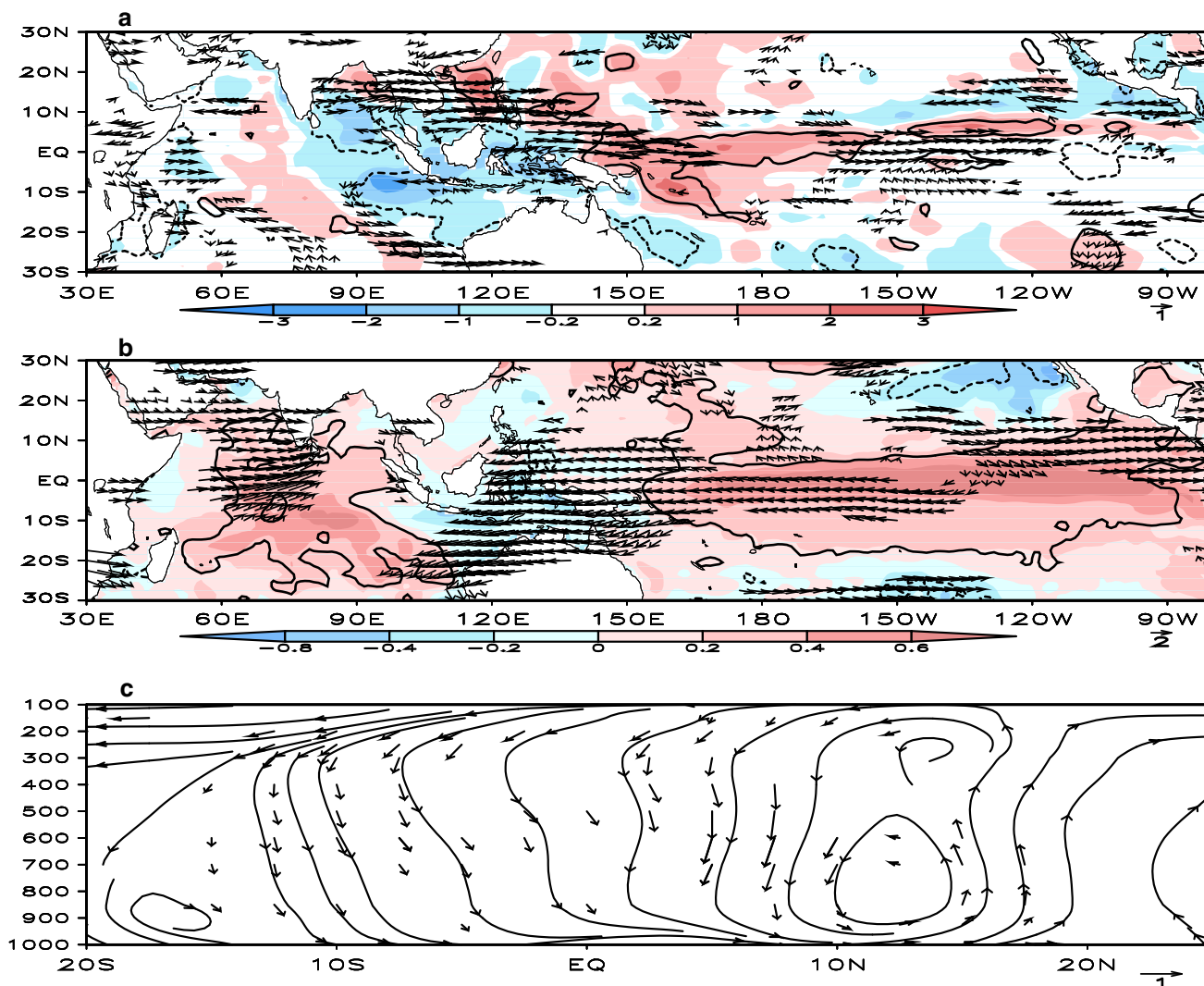


Fig. 4 JJA-mean more minus less composite anomalies for the ECP-only case of precipitation (*shading*, mm/day) and 850 hPa wind (*vector*, m/s) (a), SST (*shading*, °C) and 200 hPa wind (*vector*, m/s) (b), vertical-longitudinal circulation (unit: 10^{-2} Pa/s in vertical direction and m/s in longitudinal direction) averaged between

100°E and 130°E (c). *Thick contours* indicate that the composite anomalies are statistically significant at the 90 % confidence level. Only wind vectors that are significant at the 90 % confidence level are plotted

In response to anomalous cooling over the NIO (Fig. 5b), strong anomalous eastward flow forms from the NIO to the western North Pacific at low-level (Fig. 5a). Anomalous westward flow is seen at upper-level (Fig. 5b). This indicates that the NIO SST anomalies contribute to the variability of the SCS summer precipitation by modulating the regional east–west vertical circulation. Given negative SST anomalies in the NIO, the atmospheric column is cooled through turbulent surface heat fluxes, which induce higher surface pressure and anomalous low-level divergence (Lindzen and Nigam 1987). The corresponding anomalous cooling may in turn leads to anomalous circulation and convection in remote regions, such as the SCS and the western North Pacific. This is demonstrated in

Fig. 5c that shows the composite anomalies of zonal-vertical circulation averaged over 10°N–20°N. Following negative SST anomalies in the NIO, there is obviously an east–west vertical circulation from the NIO to the western North Pacific with anomalous descending motion between 60°E and 80°E, and anomalous ascending motion between 100°E and 140°E. This leads to above normal precipitation over northern SCS and the western North Pacific (Fig. 5a).

The role of the NIO SST anomalies in the climate variability over the western North Pacific has been discussed in previous studies (e.g., Yang et al. 2007; Xie et al. 2009). These previous studies emphasized the Kelvin wave-induced Ekman divergence mechanism. Here, our interpretation using an east–west vertical circulation provides

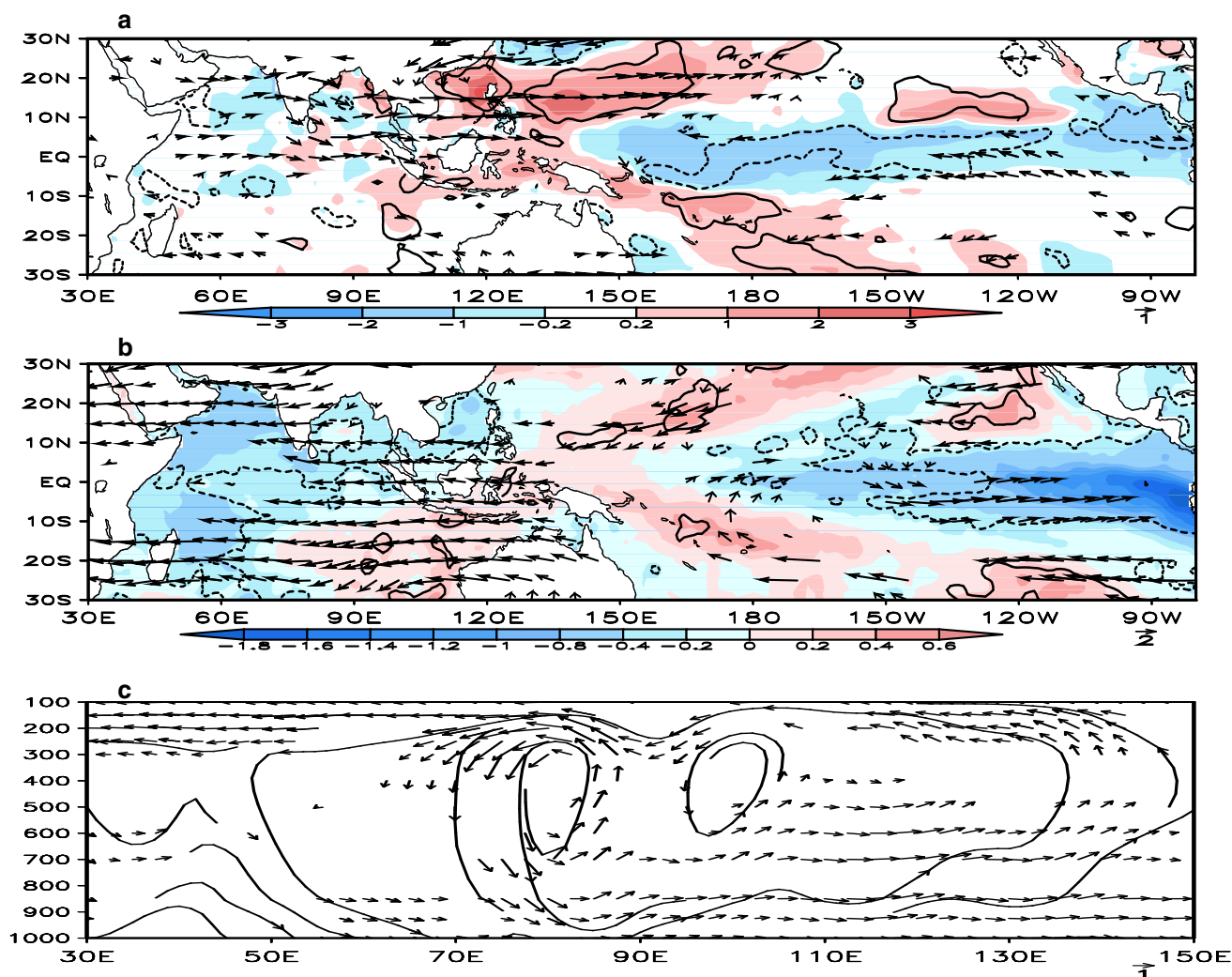


Fig. 5 JJA-mean more minus less composite anomalies for the NIO-only case of precipitation (shading, mm/day) and 850 hPa wind (vector, m/s) (a), SST ($^{\circ}\text{C}$) and 200 hPa wind (vector, m/s) (b), vertical-latitude circulation (unit: 10^{-2} Pa/s in vertical direction

and m/s in latitudinal direction) averaged between 10°N – 20°N (c). Thick contours indicate that the composite anomalies are statistically significant at the 90 % confidence level. Only wind vectors that are significant at the 90 % confidence level are plotted

an alternative mechanism for the Indian Ocean SST influence on the SCS climate. This east–west vertical circulation argument has been invoked by Wu et al. (2010) in interpreting the influence of tropical Indian Ocean warming on summer rainfall increase over southern China around 1992/93.

The anomalous low-level cyclone over the SCS and the western North Pacific also appears as a Rossby-wave type response to positive SST anomalies in the region of 10°N – 20°N , 150°E – 170°W . The above SST anomalies form an east–west SST anomaly pattern with the NIO SST anomalies. The role of the east–west SST anomaly pattern in summer SCS rainfall variability was emphasized by Wu et al. (2014). Their numerical experiments with specified SST forcing confirm the importance of the east–west SST anomaly pattern.

The Indian Ocean SST anomalies may be induced by preceding Pacific Ocean forcing (Klein et al. 1999) and thus they act as a “medium” for preceding Pacific SST influence on the SCS summer rainfall. Here, we show the correlation between the leading PC and the SST leading by 3- and 6-month (Fig. 6). Apparently, the SCS summer precipitation displays strong negative correlation with the equatorial eastern Pacific (EEP) SST in the preceding winter (Fig. 6a). This negative correlation is largely weakened in spring (Fig. 6b). For detailed examination, we calculate the normalized winter EEP SST anomalies in the region of 150°W – 90°E , 5°S – 5°N (Fig. 3). The relationship of December–February (DJF) EEP SST with the JJA NIO SST is included in Table 1. It is apparent that the NIO SST anomalies are highly coherent with the EEP anomalies with a strong tendency of same-sign relationship (Fig. 3). The

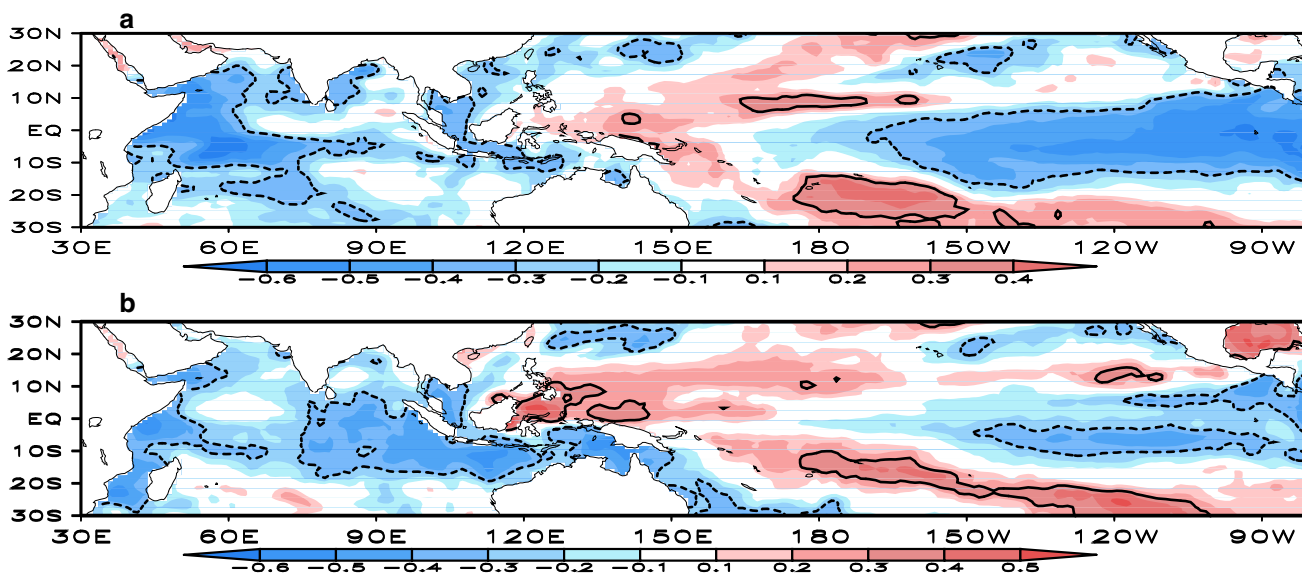


Fig. 6 Correlations between the leading PC of SCS JJA precipitation and the SST anomalies leading by 6-month (a) and 3-month (b) for the period of 1983–2012. *Thick contours* indicate that the correlation is statistically significant at the 90 % confidence level

correlation coefficients of DJF EEP SST-JJA SCS rainfall and DJF EEP SST-JJA NIO SST are -0.50 and 0.73 , respectively. In the 10 years when the NIO SST anomalies contribute to the SCS summer rainfall with an opposite-sign NIO SST-SCS rainfall relationship, there are 9 years in which an opposite-sign relationship exists between DJF EEP SST and JJA SCS rainfall (Table 1). This strongly suggests that the preceding winter Pacific Ocean SST anomalies exert an indirect/delayed influence on the SCS summer rainfall variability via the NIO SST anomalies.

The general influence of ENSO on the Indian Ocean SST anomalies has been demonstrated in previous studies (Klein et al. 1999; Lau and Nath 2003). Here, to validate the occurrence of the NIO SST anomalies in the NIO-only cases in relation to preceding winter EEP SST influence, we show in Fig. 7 the evolution of more minus less composite anomalies of short wave radiation, SST,

precipitation and vertical P-velocity from November to August. The largest negative EEP SST anomalies occur around December with the magnitude of about -1.3 °C. Through the atmospheric bridge (Klein et al. 1999; Lau and Nath 2003), the ascending motion is strengthened over the NIO from January to June with an anomalous P-velocity of about -3×10^{-3} Pa/s. The enhanced convection leads to more cloud cover, reducing the incoming solar radiation reaching the ocean surface by about 4 W/m². This contributes to a decrease in the NIO SST from April to July by about -0.4 °C. After entering the summer, the induced low SST suppresses precipitation over the NIO. This “atmospheric bridge” effect indicates that the preceding EEP SST anomalies can pose an indirect impact on the SCS summer rainfall through the Indian Ocean SST anomalies, which is different from the direct impact of concurrent ECP SST anomalies discussed in Sect. 4.1.

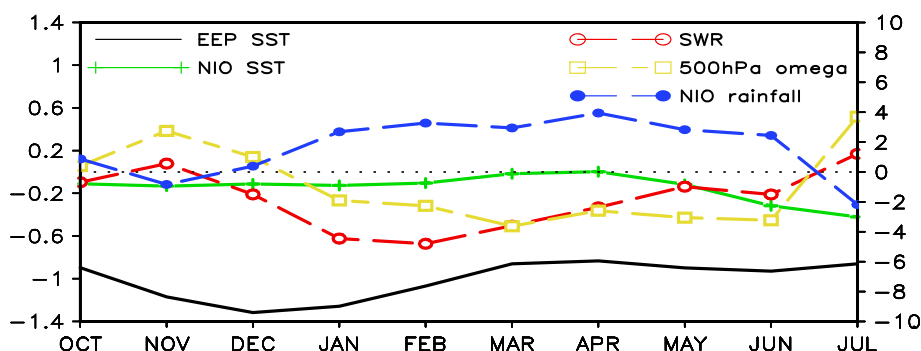


Fig. 7 The evolution of more minus less composite anomalies by a 3-month-running mean from October to the following July according to the selected years in the NIO-only case. *Scale at left* is for EEP SST

(°C), NIO SST (°C); *scale at right* is for short wave radiation (SWR, 1983 excluded for data missing, W/m²), 500 hPa vertical velocity (ω , 10^{-3} Pa/s) and precipitation (10^{-1} mm/day) in the NIO region

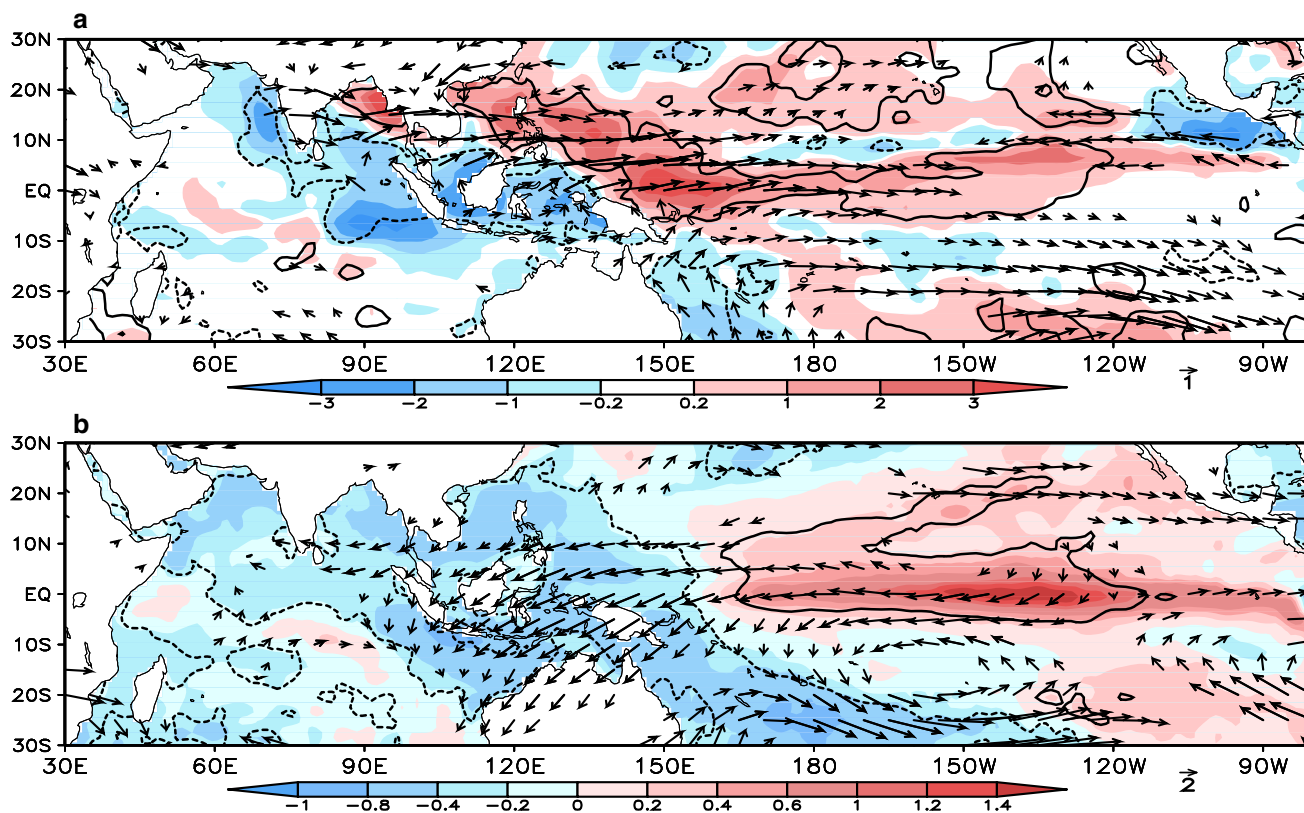


Fig. 8 JJA-mean more minus less composite anomalies for the co-existing case of precipitation (*shading*, mm/day) and 850 hPa wind (*vector*, m/s) (**a**), SST (*shading*, °C) and 200 hPa wind (*vector*, m/s)

(**b**). *Thick contours* indicate the composite anomalies are statistically significant at the 90 % confidence level. Only wind vectors that are significant at the 90 % confidence level are plotted

4.3 The co-existing ECP and NIO SST influence

Figure 8 shows composite anomalies for the 5 years (1988, 1994, 1998, 2007, and 2010) when the ECP and NIO SST influences co-exist. Both positive ECP SST anomalies and negative NIO SST anomalies can be seen in Fig. 8b. These SST anomalies have approximately the same magnitudes as those in the ECP-only cases (Fig. 4b) and the NIO-only cases (Fig. 5b), respectively. Yet, the SCS precipitation anomalies (Fig. 8a) appear more significant compared to those in the ECP-only and NIO-only forcing cases (Figs. 4a, 5a). The occurrence of precipitation anomalies over the SCS is attributed to a combined effect of both Pacific and Indian Ocean SST anomalies.

Given positive ECP SST anomalies (Fig. 8b), in the lower troposphere, prominent eastward wind anomalies prevail along tropical western and central Pacific with an anomalous cyclone extending from northern SCS to the western North Pacific (Fig. 8a). Consequently, more precipitation falls over the SCS, the Philippine Sea, and equatorial western and central Pacific. Negative SST anomalies are seen around the MC (Fig. 8b), accompanied by less precipitation (Fig. 8a). These features are similar to those in the ECP-only case. The result indicates the

contributions of both ECP and MC SST anomalies via a Rossby-wave type response and an anomalous meridional vertical circulation.

The NIO SST anomalies are significant as well. Given negative NIO SST anomalies (Fig. 8b), precipitation is reduced over the Arabian Sea and southern Bay of Bengal (Fig. 8a). Though the magnitude of the NIO SST anomalies is nearly the same as that in the NIO-only cases, the precipitation anomalies over the Arabian Sea are much larger compared to the NIO-only cases. There are anomalous low-level westerlies (Fig. 8a) and upper-level easterlies (Fig. 8b) from the Bay of Bengal to the western North Pacific. These features resemble those in the NIO-only cases. The results indicate that the NIO SST anomalies strengthen the SCS summer rainfall by modulating the east–west vertical circulation north of the equator.

5 Forced CESM experiments

In this section, numerical experiments using the CESM are conducted to address the influences of the Indo-Pacific SST forcing on the variability of SCS summer climate. Previous studies have evaluated the performance of the

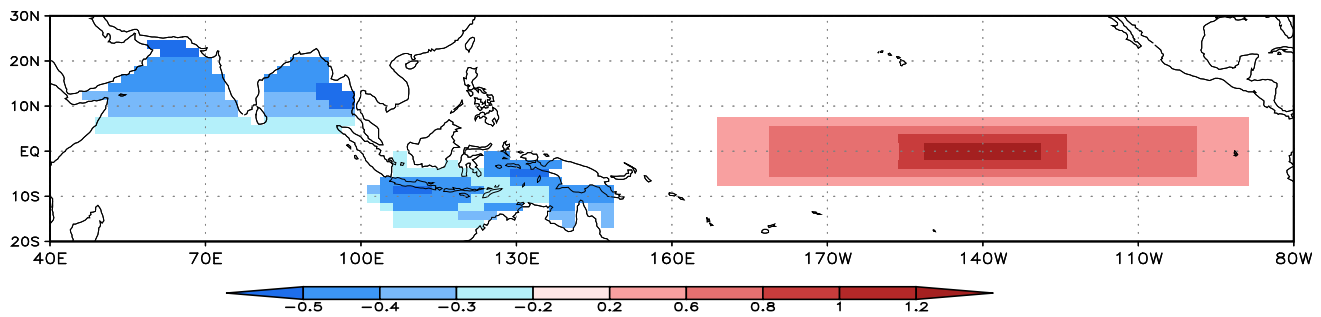


Fig. 9 Indo-Pacific SST anomalies (including the MC SST anomalies) specified as the lower boundary conditions for the positive forcing case in the numerical experiments

CESM and applied the model in the study of climate change and monsoon variability (Collins et al. 2006; Cook et al. 2012; Kay et al. 2012; Meehl et al. 2012; Muñoz et al. 2012; Neale et al. 2013). The atmospheric component of the CESM–CAM is used in the present study. Since the CAM is just a special configuration of CESM, it can be run using the CESM scripts (Eaton 2012) with default stand-alone CAM component and prescribed ocean/sea-ice component. Here, we employ regular latitude–longitude finite volume grids at a horizontal resolution of about $1.9^\circ \times 2.5^\circ$ and with 26 vertical levels. The control run is based on a 30-year integration with climatological SSTs prescribed as the lower boundary condition in the global oceanic domain. The observed climatological precipitation and atmospheric circulation during summer are well represented by the control run. Though the simulated precipitation is weaker than the observations in the eastern Indian Ocean–western Pacific region, the pattern of precipitation is highly coherent with the observations (figures not shown).

In the present study, six CESM experiments are carried out, which are divided into three groups of runs. In the ECP-forced runs, the SST forcing is specified only in the ECP region and climatological SSTs are imposed in other regions. In the NIO-forced runs, the SST forcing is prescribed only in the NIO region and climatological SSTs are imposed in other regions. While in the CO-forced runs, the SST forcing is specified in both the NIO and ECP regions. The SST forcing consists of climatological mean SST and SST anomalies. The SST anomalies in the Indo-Pacific regions (Fig. 9) are prescribed according to composite anomalies in the ECP-only case (Sect. 4.1) and the NIO-only case (Sect. 4.2). In Fig. 9, we impose the SST forcing with the ECP SST anomalies ranging from 0.2 to 1.2 °C (-0.2° to -1.2° C) as positive (negative) forcing, and the SST forcing with the NIO SST anomalies ranging from -0.2 to -0.5° C (0.2 to 0.5 °C) as the positive (negative) forcing. For both the positive and negative forcing cases, we perform ten 1-year simulations in each group.

Comparison of the forced run and the control run provides information about how the atmosphere responds to the imposed SST forcing. The differences of JJA mean between the control run and the forced runs with positive SST forcing (left figures) and negative SST forcing (right figures) are shown in Fig. 10a, b for the ECP-forced runs, Fig. 10c, d for the NIO-forced runs, and Fig. 10e, f for the CO-forced runs. During summer, precipitation and low-level wind differences display highly symmetric (with opposite signs) distributions between the positive and negative forcing cases in the ECP-forced (Fig. 10a, b) and CO-forced (Fig. 10e, f) runs.

The ECP-forced run captures well the circulation and precipitation features seen in the observational ECP-only cases. In the positive SST forcing case, low-level anomalous westerlies and above-normal precipitation prevail over the Bay of Bengal, the SCS, the western North Pacific, and equatorial central Pacific (Fig. 10a). Anomalous low-level cyclone is seen over northern SCS. These wind and precipitation anomalies feature a Rossby-wave type response to positive ECP SST anomalies as well. In the negative SST forcing case, opposite wind and precipitation anomalies are produced in the above regions (Fig. 10b).

In the NIO-forced run, the distribution of wind and precipitation anomalies displays noticeable differences between the positive and negative forcing cases (Fig. 10c, d). In the positive forcing case, negative precipitation anomalies in the NIO (Fig. 10c) are much larger than those seen in observations (Fig. 5a), likely because the specified SST simulation overestimates the atmospheric response (Wu and Kirtman 2007). An anomalous cyclone is seen over northern SCS and the western North Pacific, which is accompanied by positive precipitation over the SCS (Fig. 10c). The wind and precipitation anomalies, however, are weak. In the negative SST forcing case, an anomalous anti-cyclone is induced over 70°E – 12°E , 0°N – 20°N , which leads to less rainfall in the SCS (Fig. 10d).

In the CO-forced run, the response in the positive SST forcing case is characterized by low-level westerly

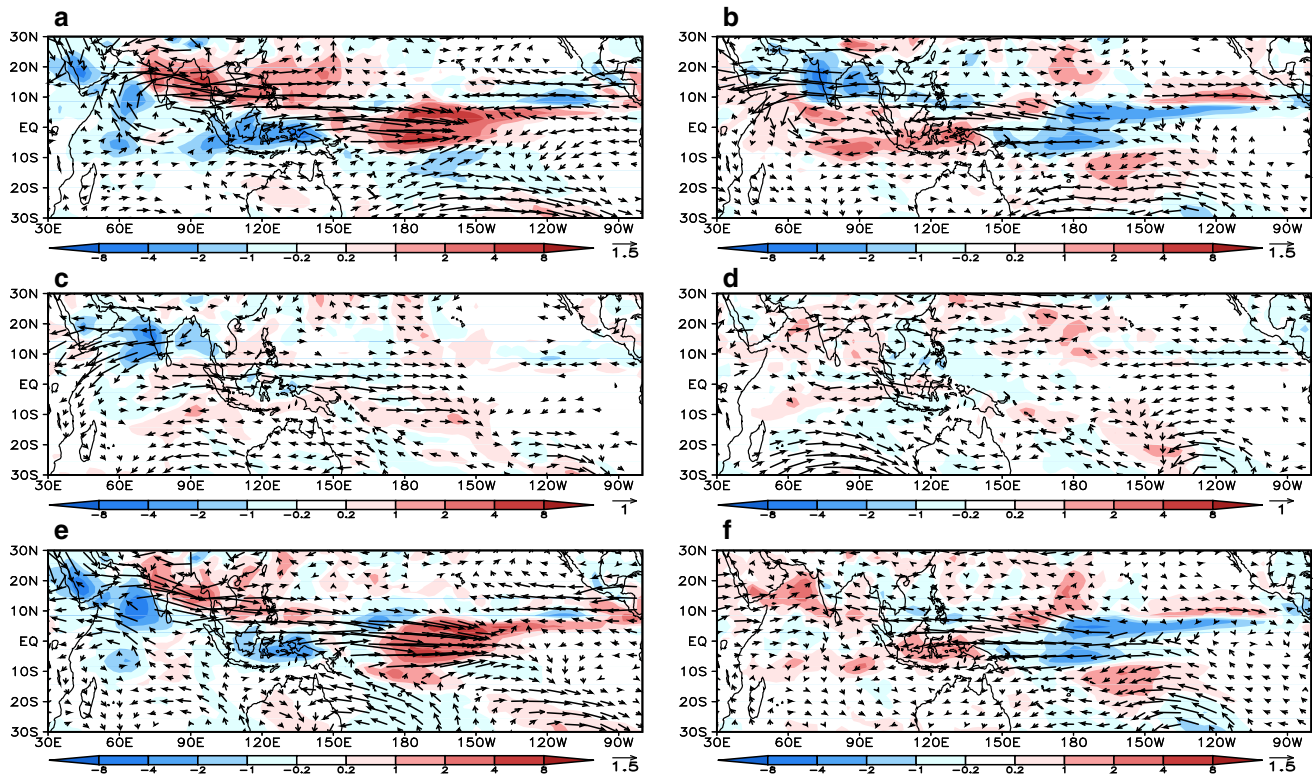


Fig. 10 The difference of JJA-mean 850 hPa wind (vector, m/s) and precipitation (shading, mm/day) between the control run and the forced runs with positive SST forcing (left panels) and negative SST

forcing (right panels): ECP-forced run (a–b), for NIO-forced run (c–d), for CO-forced run (e–f)

anomalies extending from the SCS to equatorial central Pacific with an anomalous cyclone over northern SCS and the western North Pacific (Fig. 10e). Accordingly, positive precipitation anomalies occur over northern SCS. Opposite wind and precipitation anomalies appear in the negative SST forcing case (Fig. 10f) though the magnitude of anomalies tend to be smaller over the Indian Ocean and the SCS.

The composite anomalies in observations in Sects. 4.1 and 4.3 indicate the contribution of SST anomalies around the MC to the SCS summer rainfall anomalies. Here, we conduct another experiment to confirm the impact of the MC SST anomalies. In this experiment, negative SST anomalies are specified around the MC region (Fig. 9). With these negative MC SST forcing, both northward cross-equatorial flows from the MC to the SCS and westerlies from the MC to the ECP are apparent at low-level (Fig. 11a). In the upper troposphere, anomalous convergence develops over the MC and anomalous divergence forms over the SCS and the tropical Pacific (Fig. 11b). This circulation pattern validates the modulation of negative MC SST anomalies on regional north–south and east–west circulations, which contributes to summer rainfall anomalies over northern SCS (Fig. 11a).

6 Summary and discussions

The variability of summer rainfall over the SCS is correlated with simultaneous SST anomalies in both the Indian and Pacific Ocean regions. The present study investigates the individual and combine effects of the Indian and Pacific Ocean SST forcing in the SCS summer rainfall variability and the direct and indirect influences of the Pacific SST anomalies. Both observational analyses and numerical experiments with specified SST forcing are utilized to demonstrate the influences of the Indo-Pacific SST forcing and the corresponding processes. The influences of ECP and NIO SST anomalies are distinguished by examining in detail the relationship of these SST anomalies with the SCS rainfall anomalies. Three types of cases are extracted for composite analysis: the ECP SST-only influence, the NIO SST-only influence, and the co-existing ECP and NIO SST influence. The ECP SST influence is dominant after 1990 and the NIO SST impact is relatively more important during 1980s.

In the ECP-only case, positive ECP SST anomalies induce anomalous low-level cyclone over the western North Pacific and northern SCS through a Rossby-wave type response, leading to above-normal precipitation from the equatorial Pacific to northern SCS. Meanwhile,

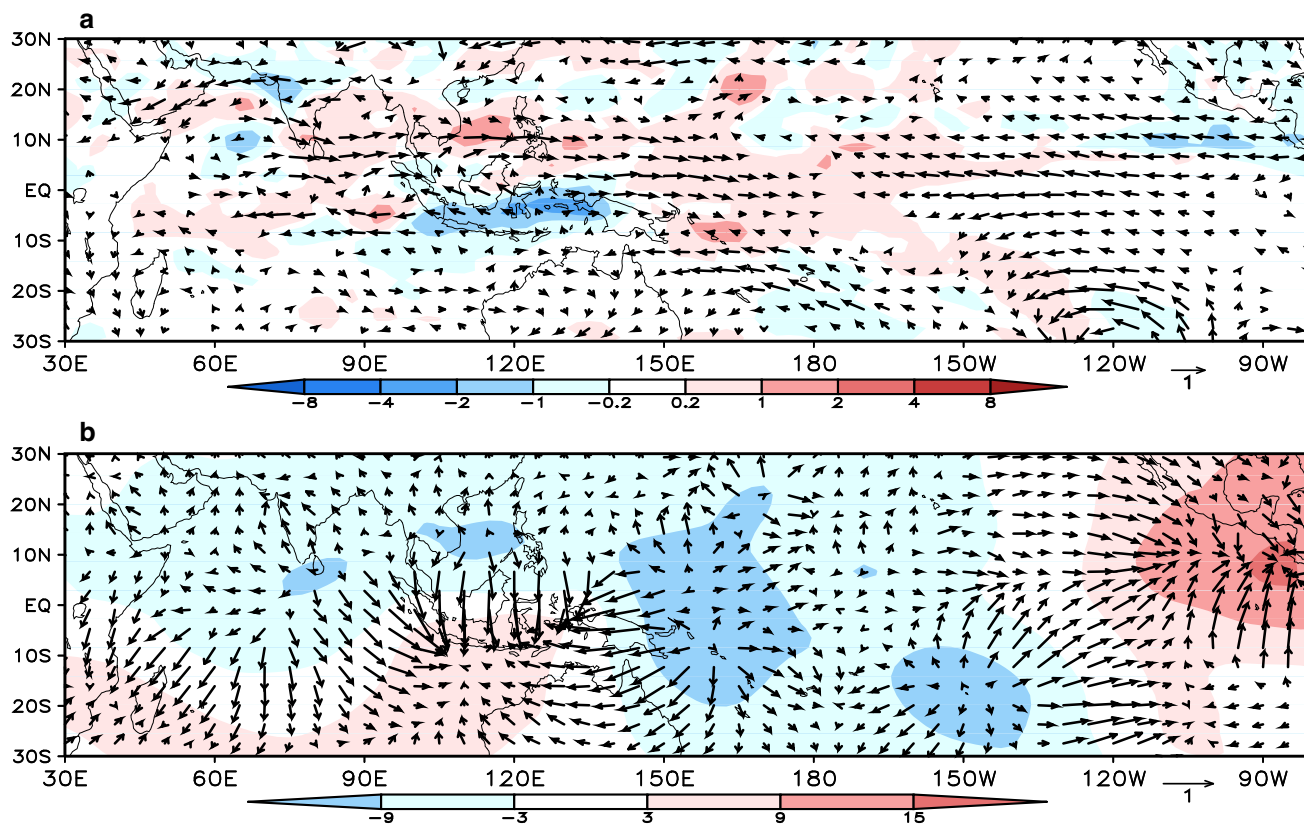


Fig. 11 The difference between the control run and the forced run with negative MC SST anomalies of JJA-mean 850 hPa wind (vector, m/s) and precipitation (shading, mm/day) (a), JJA-mean velocity potential (shading, 10^5 m²/s) and divergent wind (m/s) at 200 hPa (b)

negative MC SST anomalies work together with positive ECP SST anomalies, enhancing the SCS summer rainfall variability by modulating regional meridional and zonal vertical circulations. In the NIO-only case, the NIO SST anomalies contribute to the SCS summer rainfall variability by modulating a regional east–west vertical circulation over the NIO through the western North Pacific. The summer NIO SST anomalies are closely correlated to the EEP SST anomalies via an “atmospheric bridge”, and thus, they serve as a “medium” for an indirect impact of the preceding Pacific SST anomalies on the SCS summer rainfall variability. In the co-existing case, the ECP and NIO SST influences concur, and the occurrence of precipitation anomalies over the SCS is due to a combined effect of both the Pacific and Indian Ocean SST anomalies.

The impacts of the Indian and Pacific Ocean SST anomalies on the SCS summer rainfall variability are further investigated by numerical experiments with specified SST forcing. Based on the three types of observational cases, three groups of numerical experiments are conducted: the ECP-forced, NIO-forced, and CO-forced runs in which SST anomalies are imposed in the ECP only, the NIO only, and both regions. The experiments include both positive and negative SST forcing cases. The results of the numerical experiments are consistent with the observations,

which confirm the importance of the Indo-Pacific SST anomalies in the SCS summer rainfall variability.

The influence of the Indian and Pacific SST anomalies is discussed based on the positive minus negative composite fields. It should be stressed that the atmospheric and SST anomalies may exhibit nonlinearities between the warm and cold SST anomaly cases. The nonlinearity in the atmospheric response has been noticed in previous studies (Hoerling et al. 1997; Larkin and Harrison 2002). In the present study, owing to the limited observational samples, the nonlinearity in observations is not considered. Yet, the numerical experiments distinguish the positive and negative SST forcing cases. Based on results of numerical experiments, the ECP SST influence appears to be symmetric, whereas the NIO SST influence displays a strong nonlinearity.

As suggested in Fig. 2, the SCS summer rainfall anomalies appears to be part of a large-scale rainfall anomaly pattern encompassing most of the northwestern Pacific. To see how consistent the rainfall variations are between the SCS and Northwestern Pacific, we further examine their relationship (figures not shown). The precipitation anomalies averaged over the northern SCS and the western North Pacific region, with a correlation coefficient of 0.47, are opposite in 1991, 1995, 2004, 2006,

2008, 2011). Thus, the precipitation variations over the SCS display both coherent and different features compared to those over the northwestern Pacific. Similar mechanisms for equatorial Pacific and North Indian Ocean SST influences on the northwestern Pacific basically work for the SCS. However, it should be noted that the regional air-sea relationship displays difference between the SCS and the central North Pacific (10°N–20°N, 150°E–170°W). The SST features a response to precipitation change in the SCS, whereas in eastern part of northwestern Pacific the SST anomalies may contribute to the precipitation anomalies through a Rossby-type response by inducing an anomalous low-level cyclone (anti-cyclone). Moreover, distinguishing from previous studies on the interannual variability of the northwestern Pacific summer monsoon, our study examines the individual roles of tropical Indian and Pacific Ocean SST anomalies in the SCS—western North Pacific climate, distinguish the direct and indirect ENSO influence by considering the summer NIO SST anomalies as a “medium” of ENSO influence, consider the MC SST forcing which co-works with the CEP SST influence, and propose an alternative explanation for the NIO SST influence via an anomalous east–west circulation.

The present study mainly focuses on the influence of SST anomalies in two regions—the ECP and NIO. In addition to these two regions, the central North Pacific (150°E–170°W, 10°N–20°N) and the MC SST anomalies may also contribute to the SCS summer rainfall variability, as shown by previous studies (Wu et al. 2012, 2014; Chen et al. 2014b) and numerical experiment conducted in the present study. The role of the NIO SST anomalies as a medium for an indirect influence of preceding Pacific SST anomalies on the SCS summer rainfall variability is inferred based on the NIO SST influence on the SCS rainfall and observational evidence for the preceding Pacific SST–summer NIO SST connection. The preceding Pacific Ocean SST influence involves complicated regional air-sea interaction processes. Further experiments with coupled models need to be conducted in the future to address the impacts of preceding Pacific SST anomalies in the variability of the SCS summer climate.

Acknowledgments This study is supported by the National Basis Research Program of China grant (2014CB953902), the Hong Kong Research Grant Council Grant (CUHK403612), and the National Natural Science Foundation of China Grant (41275081).

References

- Adler RF, Huffman GJ, Chang A et al (2003) The version 2 global precipitation climatology project (GPCP) monthly precipitation analysis (1979–present). *J Hydrometeorol* 4:1147–1167
- Chen JP, Wu R, Wen ZP (2012) Contribution of South China Sea tropical cyclones to an increase in southern China summer rainfall around 1993. *Adv Atmos Sci* 29(3):585–598
- Chen Z, Wen ZP, Wu R, Zhao P, Cao J (2014a) Influence of two types of El Niños on the East Asian climate during boreal summer: a numerical study. *Clim Dyn*. doi:10.1007/s00382-013-1943-1
- Chen JP, Wen ZP, Wu R, Chen Z, Zhao P (2014b) Interdecadal changes in the relationship between Southern China winter-spring precipitation and ENSO. *Clim Dyn*. doi:10.1007/s00382-013-1947-x
- Collins WD, Rasch PJ, Boville BA et al (2006) The formulation and atmospheric simulation of the Community Atmosphere Model version 3 (CAM3). *J Clim* 19:2144–2161
- Cook KH, Meehl GA, Arblaster JM (2012) Monsoon regimes and processes in CCSM4, part 2: African and American monsoon systems. *J Clim* 25(8):2609–2621
- Ding YH (1994a) Asian monsoon. China Meteorological Press, Beijing, pp 105–113 (in Chinese)
- Ding YH (1994b) Monsoons over China. Kluwer Academic, Dordrecht
- Eaton B (2012) User’s guide to the Community Atmosphere Model CAM-5.1.1. NCAR. http://www.cesm.ucar.edu/models/cesm1.0/cam/docs/ug5_1_1/ug.html
- He ZQ, Wu R (2013a) Coupled seasonal variability in the South China Sea. *J Oceanogr* 69(1):57–69
- He ZQ, Wu R (2013b) Seasonality of interannual atmosphere–ocean interaction in the South China Sea. *J Oceanogr* 69(6):699–712
- Hoerling MP, Kumar A, Zhong M (1997) El Niño, La Niña, and the nonlinearity of their teleconnections. *J Clim* 10:1769–1786
- Huffman GJ, Adler RF, Bolvin DT, Gu G (2009) Improving the global precipitation record: GPCP version 2.1. *Geophys Res Lett* 36:L17808. doi:10.1029/2009GL040000
- Kanamitsu M, Ebisuzaki W, Woollen J, Yang SK, Hnilo JJ, Fiorino M, Potter GL (2002) NCEP–DEO AMIP-II reanalysis (R-2). *Bull Atmos Meteorol Soc* 83:1631–1643
- Kay JE, Hillman BR, Klein SA et al (2012) Exposing global cloud biases in the Community Atmosphere Model (CAM) using satellite observations and their corresponding instrument simulators. *J Clim* 25:5190–5207
- Klein SA, Soden BJ, Lau NC (1999) Remote sea surface temperature variations during ENSO: evidence for a tropical atmospheric bridge. *J Clim* 12:917–932
- Larkin NK, Harrison DE (2002) ENSO Warm (El Niño) and Cold (La Niña) event life cycles: ocean surface anomaly patterns, their symmetries, asymmetries, and implications. *J Climate* 15:1118–1140
- Lau NC, Nath MJ (2003) Atmosphere–ocean variations in the Indo-Pacific sector during ENSO episodes. *J Clim* 16:3–20
- Li CY, Zhang LP (1999) Summer monsoon activities in the South China Sea and its impacts. *Chin J Atmos Sci* 23(3):257–266 (in Chinese)
- Li S, Lu J, Huang G, Hu K (2008) Tropical Indian Ocean basin warming and East Asian summer monsoon: a multiple AGCM study. *J Clim* 21:6080–6088
- Lindzen RS, Nigam S (1987) On the role of sea surface temperature gradients in forcing low-level winds and convergence in the tropics. *J Atmos Sci* 44(17):2418–2436
- Liu QY, Jiang X, Xie SP, Liu WT (2004) A gap in the Indo-Pacific warm pool over the South China Sea in boreal winter: seasonal development and interannual variability. *J Geophys Res* 109:C07012. doi:10.1029/2003JC002179
- Meehl GA, Arblaster JM, Caron JM et al (2012) Monsoon regimes and processes in CCSM4, part 1: the Asian–Australian monsoon. *J Clim* 25(8):2583–2608

- Muñoz E, Weijer W, Grodsky SA et al (2012) Mean and variability of the tropical Atlantic Ocean in the CCSM4. *J Clim* 24(14):4860–4882
- Neale RB, Richter J, Park S et al (2013) The mean climate of the Community Atmosphere Model (CAM4) in forced SST and fully coupled experiments. *J Clim* 26(14):5150–5168
- Reynolds RW, Rayner NA, Smith TM, Stokes DC, Wang W (2002) An improved in situ and satellite SST analysis for climate. *J Clim* 15:1609–1625
- Tao SY, Chen LX (1987) A review of recent research of the East Asian summer monsoon in China. In: Chang CP, Krishnamurti TN (eds) *Monsoon meteorology*. Oxford University Press, Oxford, pp 60–92
- Verstein M, Craig T, Middleton A, Feddema D, Fischer C (2011) CESM1. 0.4 user's guide. NCAR. http://www.cesm.ucar.edu/models/cesm1.0/cesm/cesm_doc_1_0_4/x42.html
- Wang B, Zhang Q (2002) Pacific-East Asian teleconnection part II: how the Philippine Sea anomalous anticyclone is established during El Niño development. *J Clim* 15:3252–3265
- Wang B, Wu R, Fu X (2000) Pacific-East Asian teleconnection: how does ENSO affect East Asian climate? *J Clim* 13:1517–1536
- Wang B, Wu R, Li T (2003) Atmosphere–Warm Ocean interaction and its impacts on Asian–Australian monsoon variation. *J Clim* 16:1195–1211
- Wang CZ, Wang WQ, Wang DX, Wang Q (2006) Interannual variability of the South China Sea associated with El Niño. *J Geophys Res* 111:C03023. doi:10.1029/2005JC003333
- Wang GH, Su JL, Ding YH, Chen D (2007) Tropical cyclone genesis over the South China Sea. *J Mar Syst* 68:318–326
- Wu R, Kirtman BP (2007) Regimes of local air–sea interactions and implications for performance of forced simulations. *Clim Dyn* 29:393–410
- Wu R, Kirtman BP (2011) Caribbean Sea rainfall variability during the rainy season and relationship to the equatorial Pacific and tropical Atlantic SST. *Clim Dyn* 37(7–8):1533–1550
- Wu R, Wang B (2000) Interannual variability of summer monsoon onset over the western North Pacific and the underlying processes. *J Climate* 13:2483–2501
- Wu GX, Li JP, Zhou TJ et al (2006) The key regions affecting the short-term climate variations in China: the joining area of Asia and Indian-Pacific Ocean. *Adv Earth Sci* 21(11):1109–1118 (in Chinese)
- Wu R, Wen ZP, Yang S, Li Y (2010) An interdecadal change in southern China summer rainfall around 1992/93. *J Clim* 23(9):2389–2403
- Wu R, Chen J, Chen W (2012) Different types of ENSO influences on the Indian summer monsoon variability. *J Clim* 25(3):903–920
- Wu R, Huang G, Du Z, Hu K (2014) Cross-season relation of the South China Sea precipitation variability between winter and summer. *Clim Dyn*. doi:10.1007/s00382-013-1820-y
- Xie SP, Hu K, Hafner J et al (2009) Indian Ocean capacitor effect on Indo-Western Pacific climate during the summer following El Niño. *J Clim* 22:730–747
- Yang J, Liu Q, Xie SP, Liu Z, Wu L (2007) Impact of the Indian Ocean SST basin mode on the Asian summer monsoon. *Geophys Res Lett* 34:L02708. doi:10.1029/2006GL028571
- Yu L, Jin X, Weller RA (2008) Multidecade global flux datasets from the Objectively Analyzed Air–sea Fluxes (OAFlux) project: latent and sensible heat fluxes, ocean evaporation, and related surface meteorological variables. OAFlux project technical report, OA-2008-01
- Zhang Y, Rossow WB, Laci AA, Oinas V, Mishchenko MI (2004) Calculation of radiative fluxes from the surface to top of atmosphere based on ISCCP and other global data sets: refinement of the radiative transfer model and the input data. *J Geophys Res* 109:D19105. doi:10.1029/2003JD00445
- Zhou TJ, Yu RC (2005) Atmospheric water vapor transport associated with typical anomalous summer rainfall patterns in China. *J Geophys Res* 110:D08104. doi:10.1029/2004JD005413